Available online at www.sciencedirect.com
SCIENCE DIRECT®
Journal of Crystal Growth 282 (2005) 165–172
JOURNAL OF CRYSTAL GROWTH
www.elsevier.com/locate/jcrysgro

ZnO flowers made up of thin nanosheets and their optical properties

Anlian Pan, Richeng Yu, Sishen Xie, Zebo Zhang, Changqing Jin, Bingsuo Zou*

Nanoscale Physics and Device Laboratory, Institute of Physics, Chinese Academy of Sciences, Beijing 100080, China

Received 23 February 2005; accepted 1 May 2005
Available online 13 June 2005
Communicated by M. Schieber

Abstract

A new type of flower-like ZnO nanostructure was prepared on a large scale through a very simple solvothermal method. The nanoflowers are assembled by many thin and uniform hexagonal-structured ZnO nanosheets, with a thickness of around 6 nm. The growth mechanism of the nanoflowers is discussed based on the reaction conditions. Room-temperature optical measurements reveal that such ZnO nanoflowers have very strong UV bandedge emission with a large Stokes shift and an asymmetrical band profile. This luminescence characteristic may be attributed to the anisotropic energy band structure of the quantum-confined ZnO nanosheets.

PACS: 68.55.Jk; 81.05.Ys; 81.10.Dn

Keywords: A1. Crystal morphology; A2. Growth from solutions; A2. Nanostructure; B1. ZnO

1. Introduction

Nanocrystalline ZnO as a wide band semiconductor has attracted more and more attention over the past few years due to its potential applications in solar cells [1], chemical sensors [2], photocatalysis [3], optoelectronics [4], and field emission [5]. Especially zinc oxide is thought to be the most suitable material for an ultraviolet (UV) laser device due to its direct wide band gap (3.37 eV) and large exciton binding energy (60 meV). Nanosized inorganic semiconductors exhibit a wide range of electrical and optical properties, which depend sensitively on both size and shape [6,7]. Manipulation of their microstructure and morphology has aroused great interest in scientists in varied fields. Up to now, nanostructures of ZnO including prismatic, needle-like, ellipsoidal, tetrapod-like, nanorod, nanofiber, nanobelts, nanotubes, and nanocombes [8–16] have been prepared by various physical and chemical methods. Among

*Corresponding author. Tel.: +86 010 82649021.
E-mail address: zoubs@aphy.iphy.ac.cn (B. Zou).

0022-0248/$ - see front matter © 2005 Elsevier B.V. All rights reserved.
doi:10.1016/j.jcrysgro.2005.05.003

these methods, vapor–liquid–solid, chemical vapor deposition, and thermal evaporation are the three major vapor methods to fabricate these materials. However, complex procedures, sophisticated equipments, or rigid experimental conditions are involved in these vapor methods. In addition to these methods, solution chemical route including solvothermal, hydrothermal, self-assembly, and template-assisted sol–gel process has become a promising option for large-scale production of 1D nano/microscale materials due to the simple, fast, and less expensive virtues [17–22].

In addition, two-dimensional (2D) nanostructured sheets or platelets with high surface-to-volume ratio are suggested to be ideal objects for the nanoscale devices used in energy storage or conversion and data storage and memory devices [23]. Currently, much effort has been exerted to realize 2D nanostructures by controlling the sizes and shapes of inorganic solids [23–27]. However, to our knowledge, 2D nanostructured ZnO nanosheets with prominent optical properties prepared by solution chemical routes have not been reported till now. In this paper, we report a novel flower-like ZnO nanostructure prepared directly by a very simple solvothermal processing of newly prepared hydroxide colloids $Zn(OH)_2$ in anhydrous ethanol. These ZnO flowers are assembled by many very thin and uniform 2D single-crystal nanosheets with thickness of about 6 nm and show very strong UV bandedge emission.

2. Experimental procedure

In a typical process, an alkali solution of zinc hydroxide was first prepared by dissolving 0.37 g of zinc nitrate [$Zn(NO_3)_2.6H_2O$] and 0.1 g of NaOH in deionized water to form a 20 mL suspending solution. The solution was diluted to 40 mL with ethanol during magnetic stirring. Then the formed suspending solution was centrifugated and the white $Zn(OH)_2$ precipitate was obtained. Next, 40 mL anhydrous ethanol with the dispersed precipitate was put into a 100 mL beaker, which was pretreated under ultrasonic treatment for 30 min; then the mixture was transferred into a 50 mL Teflon-lined autoclave for solvothermal processing at 190 °C for 12 h in an electric desiccation box. After this process, white crystalline product (Sample 1, see Table 1) was collected by centrifugation and thorough washings with ethanol and then dried at 50 °C in air for 4 h. For comparison, other three samples under different processing conditions were obtained and examined, the results are also listed in Table 1.

The obtained sample was characterized by X-ray powder diffraction (XRD) using a Japan Rigaku D/max-2400 X-ray diffractometer equipped with graphite-monochromatized Cu Kα radiation ($\lambda = 1.54178$ A). The energy dispersive spectroscopy (EDS) and scanning electron microscope (SEM) images were achieved on a scanning electron microscope (SEM, Hitachi S-5200). The powder samples were dispersed into ethanol and then placed on the silicon wafers for SEM observation. The transmission electron microscopy images were obtained on a high-resolution transmitted electron microscopy (HRTEM, FEG-CM 200). The optical absorption of the sample was examined by Tu-1901 UV–Vis absorption spectrometer. The photoluminescence spectra (PL) were taken on a PTI-C-700 fluorescence spectrometer. A He–Cd laser line (325 nm) was used as the excitation source.

Table 1
Reaction conditions of the nanoflowers and the contrasting samples

Sample	Solvent	Ultrasonic pretreatment	Reaction type	Morphology
1	Alcohol	Yes	Solvothermal	Nanoflowers
2	Alcohol, water (volume ratio 1:1)	No	Hydrothermal	Separated nanorods
3	Alcohol, water (volume ratio 1:1)	Yes	Hydrothermal	Aggregated nanorods
4	Alcohol	No	Solvothermal	Separated nanosheets

3. Results and discussion

Fig. 1 shows the XRD pattern of the as-prepared nanoflowers. The crystallographic phase is in good agreement with the JCPDS card (36–1451) for the typical wurtzite-type ZnO crystals. The measured lattice constants of a_0 and c_0 of this hexagonal phase are 3.2555 and 5.2046 Å, respectively ($c_0/a_0 = 1.6002$). The EDS result (Fig. 2) demonstrates only elements Zn and O contained in the sample. Hence the as-prepared product is hexagonal wurtzite ZnO.

The SEM images of the sample are shown in Fig. 3. From the SEM observations, the ZnO product contains numerous flower-like aggregates

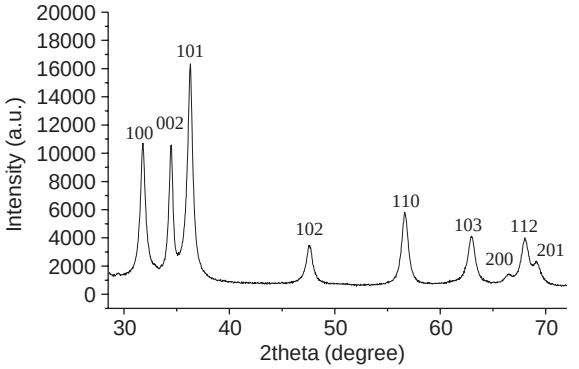

Fig. 1. XRD pattern of the as-prepared ZnO nanoflowers.

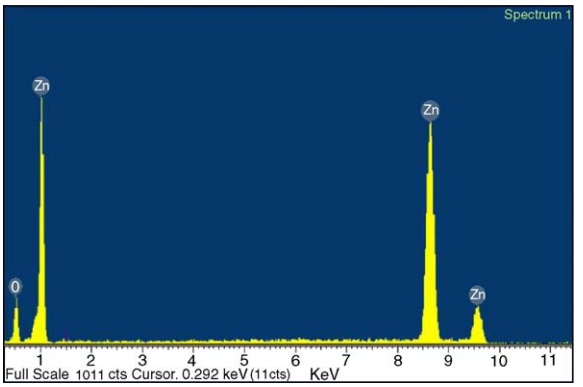

Fig. 2. Energy dispersive spectroscopy (EDS) of the as-prepared ZnO nanoflowers.

with multi-leaves, and almost all of them show same morphology. Fig. 3a and b is the image of the ZnO nanoflowers in low magnification and medium magnification, respectively. Fig. 3c is the image of a ZnO nanoflower in high magnification. From the enlarged image, each flower is made up of many thin nanosheets, which are spokewise, i.e. projected from a common central zone. Careful examination reveals that these ZnO nanosheets are 200 nm–600 nm in length and width and about 6 nm in thickness. These very thin nanosheets are responsible for the breadth of the XRD peaks (Fig. 1). Furthermore, each nanosheet has almost the same thickness perpendicular to its 2D face, indicating the sheet growth is strictly extended in the 2D plane throughout the whole growing process.

To give a further understanding of these flower-like assembles, the sample was intensively sonicated for a long time in ethanol. Many individual nanosheets and residual ZnO nanoflowers (most of the assembled nanosheets were moved off by the sonication) could be found in the sonicated sample. Fig. 4a showed the TEM image of a residual ZnO nanoflower after sonication. This image, indicated that though the flower is mainly composed of thin nanosheets, it still holds some small ZnO sprouts inserted into the body of these nanoflowers (see region B in Fig. 4a), which might grow up into large sheets. Fig. 4b is a HRTEM image corresponding to region A in Fig. 4a. It was taken with electron beam perpendicular to the extension plane of the sheet. The lattice profile can be clearly observed. The image inserted in Fig. 4b is the selected-area electron diffraction (SAED) pattern taken from the same region. The diffraction spots in this image construct rectangular arrays and the pattern can be indexed as the [1 0 0] zone of a hexagonal structure, consistent with the above XRD result. Many areas in the same sheet and in some other sheets were taken for TEM observation and the c-axis always lies in the plane of sheet (see Fig. 4b). The HRTEM and SAED observations suggested that the preferred growth directions of the nanosheets were all parallel to the [0 0 1] crystallographic direction (c-axis). These experimental results indicated that the nansosheets were grown from a different nanocrystal core at

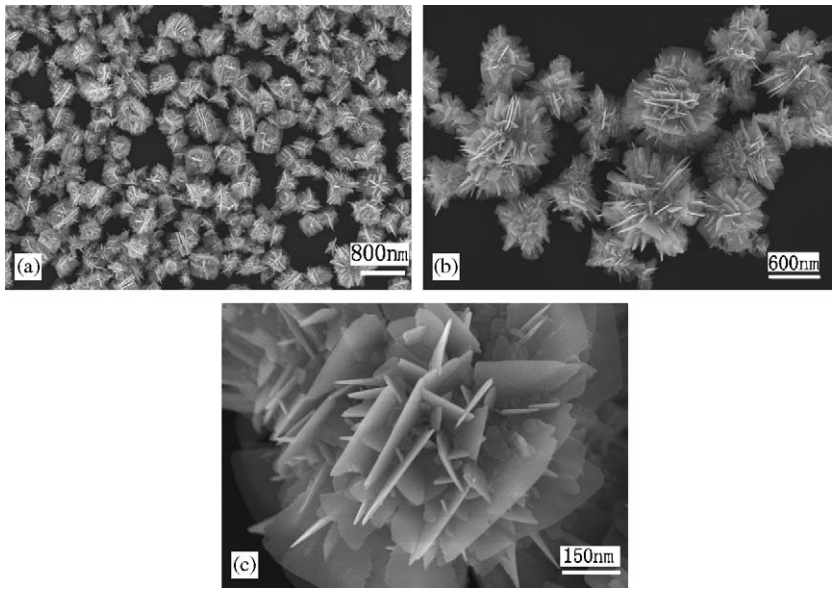

Fig. 3. SEM images of the ZnO nanoflowers in different scales: (a) and (b) is the low magnification image and medium magnification image of the ZnO nanoflowers, respectively; (c) is the high magnification image of a ZnO nanoflower.

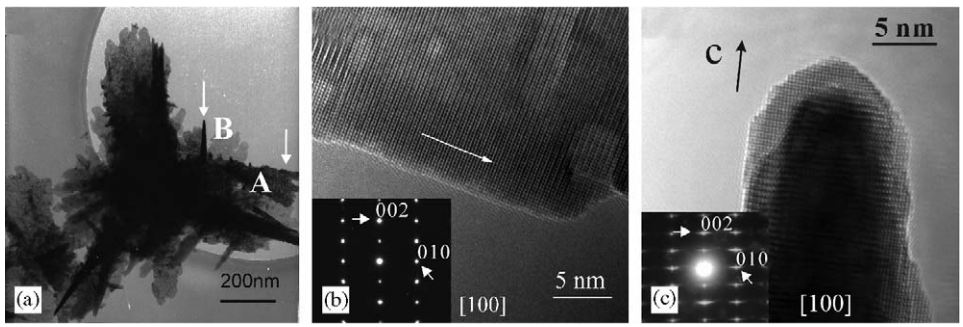

Fig. 4. TEM image of one residual ZnO nanoflower in the sonicated sample (a). (b) The HRTEM image corresponding to region A in Fig. 4a, taken with electron beam perpendicular to the wide surface of the sheet. The inset image is the selected-area electron diffraction (SAED) pattern taken from the same region. (c) The HRTEM image and SAED pattern (inset) along [1 0 0] zone, respectively, corresponding to the sprout marked with B in Fig. 4a.

the center of the flowers. Fig. 4c shows the corresponding HRTEM image and SAED pattern (the inserted image) of the sprout marked with B in Fig. 4a. Similar to Fig. 4b, Fig. 4c is also along [1 0 0] zone of the hexagonal ZnO. The HRTEM image shows its tip with only several nanometers in diameter. The growth directions in all the sprouts are along the *c*-axis from the inside of the flowers.

In contrast to the formation of ZnO nanorods in aqueous alkali solution [28], the growth in this alcohol solution shows different preference. The growth along the direction perpendicular to the *c*-axis is also permitted, but only in two directions including the *c*-axis, that is why ZnO sheets form. To investigate the formation mechanism of this ZnO flowers, we have carried out three comparison experiments (see Table 1, Samples 2–4).

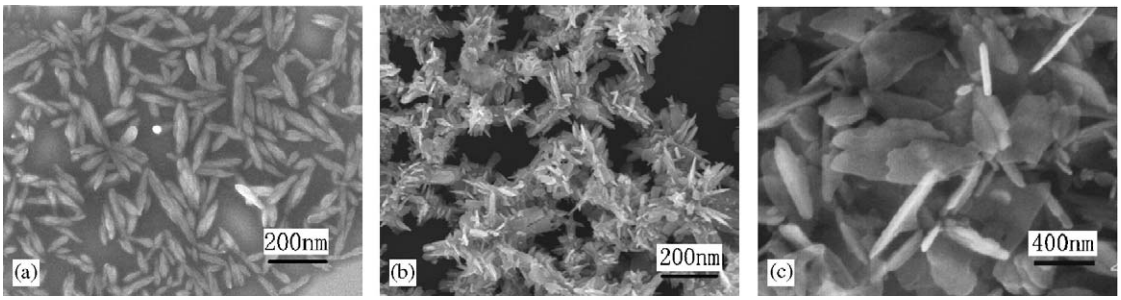

Fig. 5. The SEM images of the contrasting products prepared through the hydrothermal processing of zinc hydroxide colloid in a mixed solution of water and ethanol without (a) and with an ultrasonic pretreatment process (b), respectively. (c) The SEM image of the contrasting product prepared through the solvothermal processing of zinc hydroxide colloid in the pure ethanol solution without an ultrasonic pretreatment process.

Samples 2–4 are all pure phase hexagonal ZnO from XRD examinations. Sample 2 is short, separated nanorods (Fig. 5a), while Sample 3 is aggregated short nanorods which were assembled and extended from many growing centers (Fig. 5b), similar to those of the nanosheets in the nanoflowers (Sample 1). However, Sample 4 contains mainly the separated nanosheets, but no assembled nanoflowers were found (Fig. 5c). Therefore, the pre-sonication and a water-free circumstance are the crucial factors to obtain the nanosheet-assembled ZnO flowers.

From above data we can deduce the growth process of the ZnO flowers. There are many separated colloidal $Zn(OH)_2$ clusters in the pre-formed suspension, some of which can work as the nuclei for ZnO growth. During hydrothermal process at high temperature in aqueous alkali solution, the growth unit is $[Zn(OH)_4]$ [29]. The existence of hydroxyl groups restricts the growth of ZnO nuclei in the direction perpendicular to *c*-axis and leads to the growth along the preferred *c*-axis, then inducing the formation of many separated ZnO nanorods (Fig. 5a). In addition, sonication pretreatment of colloidal $Zn(OH)_2$ clusters generates a suitable amount of aggregates comprised of ZnO cluster nuclei for subsequent growth, since sonication can dehydrate $Zn(OH)_4$ nuclei and induce the formation of ZnO aggregations [28,30]. Each nanocluster in the aggregates has its own orientation and works as a nucleus for further growth. Thus, these nuclei develop their own preferred (*c*-axis direction) growth during the hydrothermal process. Hence the aggregates finally become the nanorod-assembles (Fig. 5b) in water. In contrast, in the pure ethanol solution, less hydroxyl groups on the surface of ZnO nuclei (without sonication) increase the packing probability of ZnO clusters at the direction including *c*-axis, making only one direction with OH restricted during growth. As a result, the separated clusters finally grow into 2D nanosheets through the high-temperature solvothermal process (Fig. 5c). Similarly, an additional ultrasonic pretreatment of the precursors in ethanol solution led to the formation of ZnO nuclei aggregates, which act as the seeds for the nanosheet-assembled ZnO flowers. The results of HRTEM and SAED examinations indicate that the preferred growth directions of the nansosheets are all along the *c* axis of the hexagonal ZnO from the center of the flowers. In addition, we also obtained similar ZnO nanosheets and nanoflowers in the pure toluene solvent, which gave a further demonstration that an anhydrous organic solution is mainly responsible for the 2D ZnO nanostructures. Fig. 6 shows the schematic growth diagram of the different ZnO nanostructures fabricated by the hydrothermal/solvothermal processes.

The optical properties of as-prepared ZnO nanoflowers at room temperature were studied. Fig. 7a illustrates the UV–Vis absorption spectrum of the nanoflowers, with a strong exciton absorption peak at 356 nm, which has a large blueshift compared to that of bulk ZnO (Fig. 7b, ~370 nm). The strong background below the peak should be

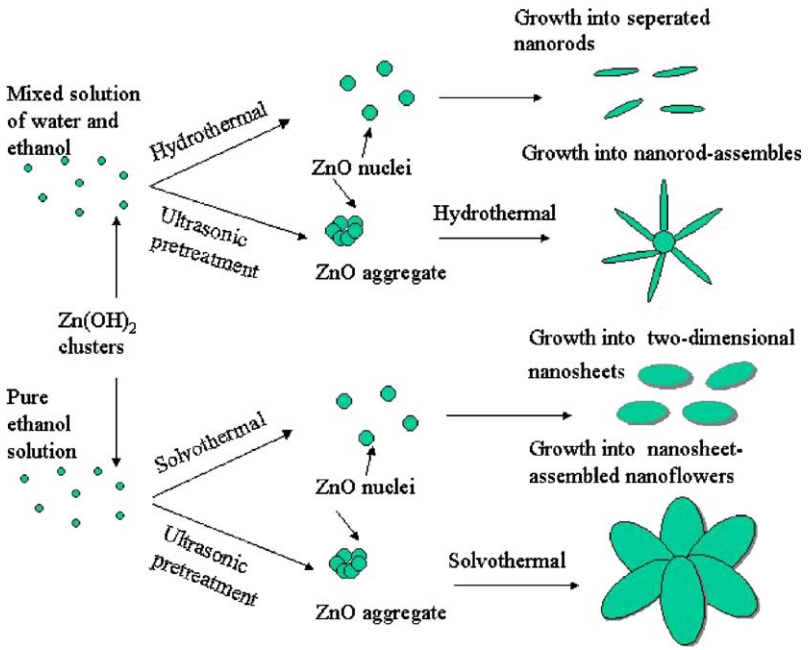

Fig. 6. The schematic growth diagram of the different ZnO nanostructures fabricated by the hydrothermal/solvothermal processes.

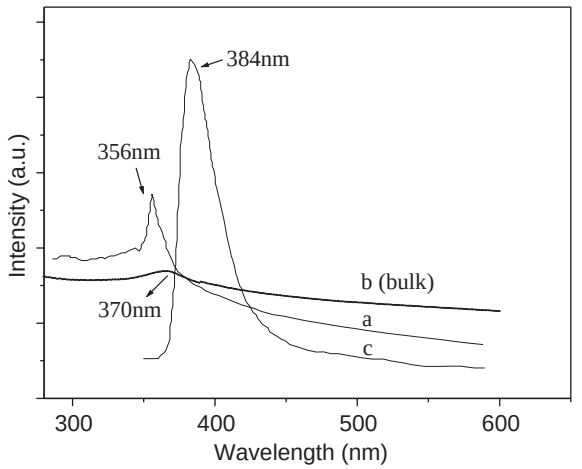

Fig. 7. UV–Vis absorption spectra of the nanosheet-assembled ZnO nanoflowers (a) and the bulk ZnO (b); the PL spectrum for the nanosheet-assembled ZnO nanoflowers (c).

due to the strong scattering of the flowers as their sizes are comparable to the light wavelength. The peak blueshift should be mainly due to the quantum confinement of the ZnO sheets, since the mean thickness of the sheets is comparable to the Bohr radius of ZnO. This confinement effect can be clearly explained using the particle energy relation of three-dimensional single-particle box [31]: $E = A\ (n_x^2/X^2 + n_y^2/Y^2 + n_z^2/Z^2)$, where A is a constant; n_x, n_y, n_z, are the quanta number; X, Y, Z are the scales in each dimension. Here for the thin ZnO nanosheets, taking the direction perpendicular to the sheet plane as the z-axis direction, the sheet plane as the $x-y$ plane, and considering the energy ground state (i.e. $n_x = n_y = n_z = 1$), then X, Y can be approximately infinite and the above energy relation can be simplified as $E = A/Z^2$. Apparently, a decreased Z value (the thickness of ZnO sheets) leads to an increased energy E. The reduction of sheet thickness produces a blueshift of the bandedge. However, why does only the direction z (but not the direction x or y) show a strong absorption peak? This is because the quantum confinement effect not only shifts the bandedge, but also enhances the exciton oscillator strength [32]. Hence the exciton along the z-direction becomes much stronger than that in $x-y$ plane. This is a good demonstration of the quantum confinement effect in the thin sheets.

Fig. 7c shows the PL spectrum of the sample excited by the He–Cd laser (325 nm line). The strong UV emission band at 384 nm was attributed to the bandedge emission of the ZnO sheets, coming from the direct recombination of the conduction band electrons and the valence band holes. The strong bandedge emission and no surface or defect related emission indicates the high crystallization of the ZnO nanoflowers, which is in agreement with the results obtained from the TEM observations. For common semiconductors, a Stokes shift in wavelength (<20 nm) between the spectral positions of the band maxima of the absorption and luminescence is usually observed due to energy transfer or lattice vibration and the emission band should be symmetrical Gaussian profile. The exceptionally large Stokes shift ($\sim$28 nm) and the asymmetrical emission band profile in the nanosheet-assembled flower-like sample indicates the existence of the anisotropic energy band structure of the very thin ZnO nansosheets. That is to say, the absorption peak of 356 nm is originated from exciton along the z-axis (i.e. the direction perpendicular to the plane of sheet) but the emission may occur mainly along the direction parallel to z (i.e. the direction along the plane of sheet) for their low energy level. This anisotropy can be used to account the large Stokes shift and asymmetrical band profile. Such optical processes can also explain why the peak position of the emission band has no apparent blueshifts as compared to that of bulk ZnO ($\sim$380 nm). Further experimental evidences are needed to support this deduction.

4. Conclusion

A type of flower-shaped ZnO nanostructure was achieved on a large scale in a relatively pure ethanol circumstance through a very simple solvothermal method. The nanoflowers are assembled by many hexagonal-structured ZnO nanosheets, which are very thin and uniform with the thickness of around 6 nm.The growth mechanism of the nanoflowers is analyzed. This finding helps to proceed the fabrication of other novel nanostructure materials only through this facile hydrothermal/solvothermal route. The ZnO nanoflowers show very strong bandedge emission at room temperature with an exceptionally large Stokes shift and an asymmetrical emission band, which is attributed to the strong quantum confinement and anisotropic energy band structure of the very thin ZnO nanosheets. This particular optical property may have potential significance in future scientific research and application.

Acknowledgments

The authors thank the financial supports of NSFC of China (Term no. 20173073), National 973 project (2002CB713802), and Nanodevice key project of CAS.

References

[1] K. Hara, et al., Sol. Energy Mater. Sol. Cells 64 (2000) 115.
[2] J.A. Rodriguez, T. Jirsak, J. Dvorak, S. Sambasivan, D. Fischer, J. Phys. Chem. B 104 (2000) 319.
[3] H. Yumoto, T. Inoue, S.J. Li, T. Sako, K. Nishiyama, Thin Solid Films 345 (1999) 38.
[4] M.H. Huang, S. Mao, H. Feick, H. Yan, Y. Wu, H. Kind, E. Weber, R. Russo, P. Yang, Science 292 (2001) 1897.
[5] C. Liu, J.A. Zapien, Y. Yao, X. Meng, C.S. Lee, S. Fan, Y. Lifshitz, S.T. Lee, Adv. Mater. 15 (2003) 838.
[6] X. Chen, A. Nazzal, D. Goorskey, M. Xiao, Phys. Rev. B 64 (2001) 245304.
[7] Z.L. Xin, B.X. Jian, Phys. Rev. B 66 (2002) 115316.
[8] W.J. Li, E.W. Shi, W.Z. Zhong, Z. Yin, J. Crystal Growth 203 (1999) 186.
[9] C. Lu, C. Yeh, Ceram. Int. 26 (2000) 351.
[10] C.H. Hung, W.T. Whang, J. Crystal Growth 268 (2004) 242.
[11] V.A.L. Roy, A.B. Djurisic, W.K. Chan, J. Gao, H.F. Liu, C. Surya, Appl. Phys. Lett. 83 (2003) 141.
[12] J.B. Baxter, F. Wu, E.S. Aydil, Appl. Phys. Lett. 83 (2003) 3797.
[13] Z.Q. Li, Y.J. Xiong, Y. Xie, Inorg. Chem. 42 (2003) 8105.
[14] Z.W. Pan, Z.R. Dai, Z.L. Wang, Science 291 (2001) 1947.
[15] J.Q. Hu, Y. Bando, Appl. Phys. Lett. 82 (2003) 1401.
[16] H. Yan, R. He, J. Johnson, M. Law, R.J. Saykally, P. Yang, J. Am. Chem. Soc. 125 (2003) 4728.
[17] L.E. Greene, L. Matt, G. Joshua, K. Franklin, J.C. Johnson, Y.F. Zhang, R.J. Saykally, P.D. Yang, Angew. Chem., Int. Ed 42 (2003) 3031.
[18] L. Vayssieres, Adv. Mater. 15 (2003) 464.
[19] D.S. Boyle, K. Govender, P. O'Brien, Chem. Commun. 15 (2002) 80.
[20] S. Yamabi, H. Imai, J. Mater. Chem. 12 (2002) 3773.

[21] K. Govender, D.S. Boyle, P. O'Brien, D. Binks, D. West, D. Coleman, Adv. Mater. 14 (2002) 1221.
[22] L. Vayssieres, K. Keis, A. Hagfeldt, S.E. Lindquist, Chem. Mater. 13 (2001) 4395.
[23] H. Ng, et al., Science 300 (2003) 1249.
[24] S.H. Yu, M. Yoshimura, Adv. Mater. 14 (2002) 296.
[25] Y.C. Zhu, Y. Bando, Chem. Phys. Lett. 372 (2003) 640.
[26] J.Q. Hu, Y. Bando, J.H. Zhan, Y.B. Li, T. Sekiguchi, Appl. Phys. Lett. 83 (2003) 4414.
[27] J. Tanori, M.P. Pileni, Langmuir 13 (1997) 639.
[28] B. Liu, H. Zeng, J. Am. Chem. Soc. 125 (2003) 4430.
[29] H. Zhang, D. Yang, X. Ma, Y. Ji, J. Xu, D. Que, Nanotechnology 15 (2004) 622.
[30] D. Qian, J.Z. Jiang, P.L. Hansen, Chem. Commun. 9 (2003) 1078.
[31] J.Y. Zeng, Introduction to Quantum Mechanics, Peking University Press, Beijing, 1991.
[32] E. Hanamura, Phys. Rev. B 37 (1988) 1273.